Thermoelectric characterization of the clathrate-I solid solution Ba8–δAuxGe46–x

Michael Baitinger, Hong Duong Nguyen, Christophe Candolfi, Iryna Antonyshyn, Katrin Meier-Kirchner, Igor Veremchuk, Valeriy Razinkov, Mykola Havryluk, Raul Cardoso-Gil, Ulrich Burkhardt, et al.

Applied Physics Letters ARTICLE scitation.org/journal/apl

Thermoelectric characterization of the clathrate-I solid solution $Ba_{8-\delta}Au_xGe_{46-x}$

Cite as: Appl. Phys. Lett. **119**, 063902 (2021); doi: 10.1063/5.0059166
Submitted: 7 June 2021 · Accepted: 11 July 2021 ·
Published Online: 12 August 2021

Michael Baitinger,[1,a)] Hong Duong Nguyen,[2] Christophe Candolfi,[3] Iryna Antonyshyn,[1] Katrin Meier-Kirchner,[1] Igor Veremchuk,[4] Valeriy Razinkov,[5] Mykola Havryluk,[5] Raul Cardoso-Gil,[1] Ulrich Burkhardt,[1] Bodo Böhme,[1] Lukyan Anatychuk,[5] and Yuri Grin[1]

AFFILIATIONS

[1]Max-Planck-Institut für Chemische Physik fester Stoffe, Nöthnitzer Str. 40, 01187 Dresden, Germany
[2]Enviromental and Resources Management Department, Quang Ninh Economic Zone Authority, Ha Long City, Vietnam
[3]Institut Jean Lamour, UMR 7198 CNRS – Université de Lorraine, Campus ARTEM, 2 allée André Guinier, BP 50840, 54011 Nancy, France
[4]Helmholtz-Zentrum, Dresden-Rossendorf, Bautzener Landstraße 400, 01328 Dresden, Germany
[5]Institute of Thermoelectricity, NAS and MES, Nauky str. 1, 58000 Chernivtsi, Ukraine

Note: This paper is part of the APL Special Collection on Thermoelectric Materials Science and Technology Towards Applications.
[a)]**Author to whom correspondence should be addressed:** Michael.Baitinger@cpfs.mpg.de

ABSTRACT

Clathrate-I-based materials are promising for waste-heat recovering applications via thermoelectric (TE) effects. However, the lack of highly efficient *p*-type materials hampers the development of clathrate-based TE devices. In this work, the synthesis of the *p*-type semiconductor $Ba_{7.8}Au_{5.33}Ge_{40.67}$ with clathrate-I structure is up-scaled by steel-quenching and spark plasma sintering treatment at 1073 K. A thermoelectric figure of merit $ZT \approx 0.9$ at 670 K is reproducibly obtained, and 40 chemically homogeneous module legs of $5 \times 5 \times 7\ mm^3$ are fabricated. By using a carbon layer as a diffusion barrier, electrical contacts are sustainable at elevated application temperatures. Eight couples with the clathrate-I compounds $Ba_{7.8}Au_{5.33}Ge_{40.67}$ as *p*-type and $Ba_8Ga_{16}Ge_{30}$ as *n*-type materials are integrated into a TE module with an output power of 0.2 W achieved under a temperature difference $\Delta T = 380$ K ($T_1 = 673$ K and $T_2 = 293$ K). The thermoelectric performance of $Ba_{7.8}Au_{5.33}Ge_{40.67}$ demonstrates the potential of type-I clathrates for waste heat recycling.

Type-I clathrates consist of a host framework enclosing guest atoms in polyhedral cages. The structure type occurs for various inorganic compounds ranging from gas hydrates to silicates and intermetallic clathrates.[1,2] In the latter, the host framework typically comprises group 14 elements encapsulating electropositive metal atoms. In addition to the examples with a homoatomic framework such as Na_8Si_{46},[3] group 14 elements can partially be replaced by four-bonded group 13 elements like in $Ba_8Ga_{16}Ge_{30}$,[4] by *d*-elements like in $Ba_{8-\delta}Au_{5.33}Ge_{40.67}$,[5] or by framework vacancies.[6,7] Intermetallic clathrates generally feature modifiable chemical compositions and, independent from that, a low lattice contribution to heat conductivity. Both features are favorable for the design of thermoelectric materials, requiring a high Seebeck coefficient α, a low electrical resistivity ρ, and a low thermal conductivity κ, summarized in the thermoelectric figure of merit $ZT = \alpha^2 T/\rho\kappa$. In application, thermoelectric properties also depend on the microstructure such as the grain size or the composition of impurity phases segregated at grain boundaries. For this reason, bulk materials do not always reflect the intrinsic properties of a substance, and *ZT* values of reported compounds may differ substantially. In this regard, for the clathrate-I phase $Ba_8Au_xGe_{46-x}$, different results were reported. At composition $Ba_8Au_{5.33}Ge_{40.67}$, a maximum *ZT* value of 0.9 was found at 700 K,[8] still the highest value obtained for a clathrate with *p*-type electrical conduction. In another study, however, a much lower maximum *ZT* value of 0.4 was achieved at 800 K for the composition $Ba_8Au_6Ge_{40}$.[9] In this work, we have achieved a reproducible material characterization and optimized the chemical composition to obtain legs suitable for thermoelectric module manufacturing.

In the ternary Ba–Au–Ge system, the clathrate-I type has been reported for compositions ranging from $Ba_8Ge_{43}\square_3$ to $Ba_8Au_6Ge_{40}$ (□ stands for framework vacancy).[9] For the series $Ba_8Au_xGe_{46-x}$,

samples showed *n*-type electrical conduction for $x \leq 5.0$ switching to *p*-type for $x \geq 5.25$.[10] Recently, a single-crystalline specimen grown by the Bridgeman method revealed the composition $Ba_{7.8}Au_{5.33}Ge_{40.67}$,[5] where the cubic clathrate-I structure with space group *Pm*-3*n* is formed by a framework of 5.33 Au and 0.67 Ge_1 atoms at Wyckoff position 6*c*, 16 Ge_2 atoms at 16*i*, and 24 Ge_3 atoms at 24*k* (Fig. 1). The framework atoms form pentagonal–dodecahedral cages fully occupied by Ba1 atoms at position 2*a*, and tetrakaidecahedral cages partially occupied by 5.8 Ba2 atoms at position 6*d*. The substitution of a Ge atom in the four-bonded framework by Au ($d^{10}s^1$ configuration) formally requires additional three valence electrons to generate four two-center-two-electron Au–Ge bonds. Within this Zintl-like interpretation, the composition $Ba_8Au_{5.33}Ge_{40.67}$ is charge-balanced: $[Ba^{2+}]_8[(4b)Au^{3-}]_{5.33}[(4b)Ge^0]_{40.67}$. The actual composition $Ba_{7.8}Au_{5.33}Ge_{40.67}$ formally implies an electron balance $[Ba^{2+}]_{7.8}[(4b)Au^{3-}]_{5.33}[(4b)Ge^0]_{40.67} \times 0.4\ h^+$, which is consistent with the *p*-type electrical conduction observed experimentally.[8]

Sample preparation was performed on a 100 g scale with techniques allowing for sufficiently high throughput. In the first step, a precursor alloy with target composition was prepared from BaGe, Au, and α-Ge in a dry, Ar-filled glovebox. Batches of 3 g were melted at 1400 K in an open glassy-carbon crucible (Sigradur, MKS, ∅ = 12 mm, *l* = 20 mm) by using an induction furnace and rapidly cooled by pouring the melt onto a steel plate and hammering.[2,11] Afterward, the glassy carbon crucibles remained shiny and did not show visible signs of a reaction with the melt. By reacting the binary precursor phase BaGe[12] instead of elemental barium, the reaction is less exothermic, enabling the use of an open crucible without material loss by squirting. Nevertheless, at temperatures of about 1300 K, which were applied to obtain a homogenous melt [melting point of the clathrate phase is 1204 K (Ref. 8)], a loss of barium by evaporation could not be avoided entirely. Thus, an excess of Ba was required to obtain a single-phase material. The microstructure of a sample with nominal composition $Ba_{8.1}Au_{5.33}Ge_{40.67}$ did not show any minority phases after steel quenching and after further annealing at 1073 K (Fig. S1). The x-ray powder diffraction (XRPD) pattern is in agreement with the reported structure model of $Ba_{7.8}Au_{5.33}Ge_{40.67}$ (Fig. S2).[5] In contrast, a sample with the slightly different nominal composition $Ba_8Au_{5.33}Ge_{40.67}$ showed inclusions of α-Ge, while in samples with higher Au contents, e.g., $Ba_8Au_6Ge_{40}$, the phase $BaAu_xGe_{4-x}$ appeared at composition $BaAu_{1.1}Ge_{2.9}$ (Ref. 9) as a minority phase.

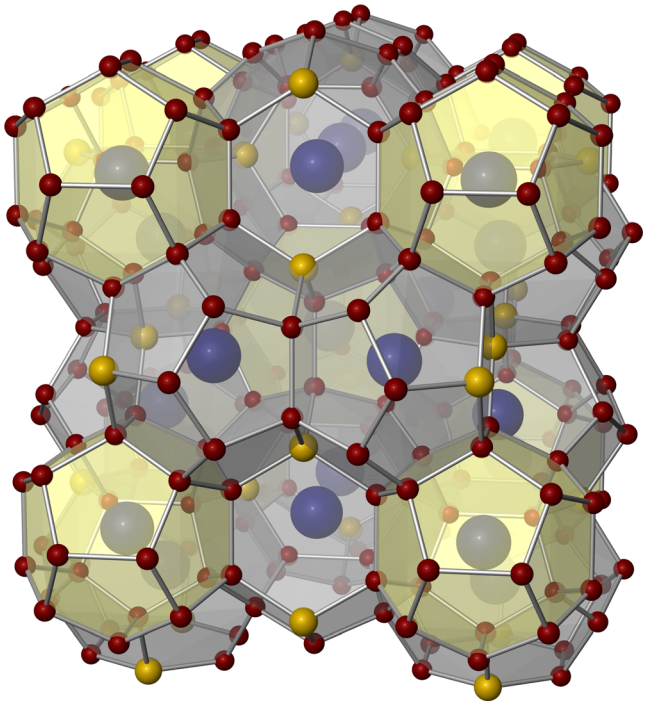

FIG. 1. Cubic clathrate-I structure of $Ba_{8-\delta}Au_xGe_{46-x}$ ($x \leq 6$) with space group *Pm*-3*n*. Barium atoms (blue spheres) occupy 20-atom (yellow) and 24-atom cages (grey), gold atoms in the framework are accentuated by golden, and germanium atoms by red spheres.

In order to manufacture module legs, the as-cast samples were ground and sieved to a grain size of $d \leq 100\ \mu m$, and the powder was compressed by spark-plasma sintering (SPS) at 1073 K to cylindrical pellets with 98% of XRD density. During the sintering process, the samples were wrapped by a carbon foil. After SPS treatment, the pellets were further annealed for seven days at 1073 K in glassy carbon crucibles sealed in tantalum ampoules. After this additional annealing step, the change in lattice parameter was not significant, indicating that the conversion of the reactants after SPS was completed (Table I). After SPS treatment, the microstructure showed pronounced grain boundaries (Fig. 2) and minority phases α-Ge and $BaAu_{1.1}Ge_{2.9}$ below the detection level of XRD. Finally, the SPS sintered pellets were diced on air with a diamond wire saw into blocks of $5 \times 5 \times 7\ mm^3$ for integration into a thermoelectric module.

Thermoelectric properties were studied for two series of compositions. The electrical conductivity and the Seebeck coefficient were measured simultaneously by using a ZEM-3 instrument (ULVAC-RIKO), while the thermal diffusivity λ was determined using the laser flash technique (LFA 447 Micro Flash, Netzsch). The thermal conductivity κ was calculated subsequently from the relationship $\kappa \approx C_p\ d\ \lambda$, where d is the sample density and C_p is the specific heat capacity. The latter was estimated according to the Dulong–Petit law. The first series, $Ba_{8.1}Au_xGe_{46-x}$, was expected to result in the single-phase material, which was the case for samples in the range $5.25 \leq x \leq 5.38$. In this series, samples with $x \geq 5.41$ showed $BaAu_{1.1}Ge_{2.9}$ (Ref. 9) as a by-product (Table I). A second series with nominal composition $Ba_8Au_xGe_{46-x}$ was prepared to investigate the influence of excess-amounts of α-Ge at the grain boundaries on the thermoelectric performance. While the lattice parameter of samples in the series $Ba_{8-\delta}Au_xGe_{46-x}$ was found to increase linearly with *x* for $0 < x < 5$,[9] the differences for the chosen composition range were found to be smaller than 2×10^{-3} Å, indicating that the change in the thermoelectric properties could not be traced by x-ray diffraction. Nevertheless, in both sample series, the development of the thermoelectric properties was controlled by the nominal sample composition.

The temperature dependence of the electrical resistivity ρ systematically varies as a function of the Au content [Figs. 3(a) and 3(e)]. It reaches a maximum at the nominal composition $Ba_8Au_{5.25}Ge_{40.75}$, which fits the composition $Ba_8Au_{5.33}Ge_{40.67}$ predicted by the Zintl–Klemm concept, where semiconducting properties are expected. The validity of the Zintl–Klemm formalism as a rule of thumb to predict the evolution of the electronic properties has also been verified for the related Ba–Au–Si type-I clathrates.[13,14] Consistently with the

TABLE I. Constituting phases and lattice parameters of the clathrate-I phase (C-I) in samples with nominal composition $Ba_{8.1}Au_xGe_{46-x}$ and $Ba_8Au_xGe_{46-x}$. Phase analysis was performed by XRPD and energy dispersive x-ray spectroscopy.

Nominal composition	Phases detected	a/Å
$Ba_{8.1}Au_{5.25}Ge_{40.75}$	C-I	10.7992(2)
$Ba_{8.1}Au_{5.30}Ge_{40.70}$		10.7994(2)
$Ba_{8.1}Au_{5.35}Ge_{40.65}$		10.7991(2)
$Ba_{8.1}Au_{5.38}Ge_{40.62}$		10.7985(2)
$Ba_{8.1}Au_{5.41}Ge_{40.59}$	C-I + $BaAu_{1.1}Ge_{2.9}$	10.7981(2)
$Ba_{8.1}Au_{5.44}Ge_{40.56}$		10.7983(2)
$Ba_{8.1}Au_{5.47}Ge_{40.53}$		10.7983(2)
$Ba_{8.1}Au_{5.50}Ge_{40.50}$		10.7983(2)
$Ba_{8.1}Au_{5.53}Ge_{40.47}$		10.7983(2)
$Ba_{8.1}Au_{5.56}Ge_{40.44}$		10.7978(2)
$Ba_{8.1}Au_{5.65}Ge_{40.35}$		10.7970(2)
$Ba_{8.1}Au_{6.05}Ge_{39.95}$		10.7973(2)
$Ba_8Au_{5.20}Ge_{40.80}$	C-I + α-Ge	10.7994(2)
$Ba_8Au_{5.25}Ge_{40.75}$		10.7992(2)
$Ba_8Au_{5.30}Ge_{40.70}$		10.7990(2)
$Ba_8Au_{5.33}Ge_{40.67}$		10.7992(1)
$Ba_8Au_{5.36}Ge_{40.64}$		10.7981(2)
$Ba_8Au_{5.39}Ge_{40.61}$		10.7984(1)
$Ba_8Au_{5.42}Ge_{40.58}$		10.7976(2)
$Ba_8Au_{5.45}Ge_{40.55}$		10.7983(2)
$Ba_8Au_{5.48}Ge_{40.52}$		10.7966(2)
$Ba_8Au_{5.51}Ge_{40.09}$	C-I + $BaAu_{1.1}Ge_{2.9}$	10.7967(2)

expected semiconducting behavior, $\rho(T)$ decreases with increasing temperature for the compositions with $x = 5.20$, 5.25, and 5.30 for the series $Ba_8Au_xGe_{46-x}$ and $x = 5.35$ for the series $Ba_8Au_xGe_{46-x}$. For the series $Ba_{8.1}Au_xGe_{46-x}$, the observed decrease starting above 500 and 600 K for $x = 5.35$ and 5.25, respectively, is due to minority carrier activation. Common to both series is the emergence of degenerate semiconducting behavior for $x > 5.35$ induced by an increase in the carrier concentration controlled by x. Samples of the series $Ba_8Au_xGe_{46-x}$ with Ge excess generally feature higher ρ values than samples of the series $Ba_{8.1}Au_xGe_{46-x}$ with $BaAu_xGe_{4-x}$ by-product. The presence of α-Ge at the grain boundaries may lead to stronger charge carrier scattering and, hence, reduced charge carrier mobility.

The thermopower α generally correlates with the electrical resistivity of the samples. In this case, samples of the series $Ba_8Au_xGe_{46-x}$ with higher electrical resistivity show higher α values compared to the series $Ba_{8.1}Au_xGe_{46-x}$ [Figs. 3(b) and 3(f)]. For both series, the prevailing n-type conduction in the composition range $5.20 \leq x \leq 5.25$ switches to a p-type behavior for higher Au concentrations. The high α values measured for the n- (up to $-200\,\mu V\,K^{-1}$ at 300 K) and p-type samples with the lowest Au contents (up to $+400\,\mu V\,K^{-1}$ at 300 K) are consistent with lightly doped semiconducting behavior. These samples show a broad maximum in $\alpha(T)$ between 400 and 550 K followed by decaying α values due to the thermal activation of minority carriers that dominate transport. From the maximum temperature T_{max} and associated α_{max} values, band gaps of $E_g = 0.2$ eV can be inferred according to the Goldsmid-Sharp relation $E_g = 2eT_{max}\alpha_{max}$. This value is in very good agreement with electronic band structure calculations performed for the composition $Ba_8Au_6Ge_{40}$ and with prior experimental results.[8] Progressively increasing Au concentration results in a monotonic decrease in the α values and in $\alpha(T)$ that follow linear temperature dependences, as expected for degenerate semiconductors.

The total thermal conductivity κ is low for all samples, ranging between 0.75 and 1.5 $W\,m^{-1}\,K^{-1}$ at 300 K [Figs. 3(c) and 3(g)]. The increase observed above 500 K in several samples of both series is due to the thermal activation of minority carriers across the bandgap that gives rise to an additional bipolar contribution. Below this temperature, κ is the sum of a phonon contribution κ_L and an electronic contribution κ_e that can be estimated using the Wiedemann–Franz law $\kappa_e = LT/\rho$, where L is the Lorenz number. Because κ_e is inversely proportional to the electrical resistivity, the non-degenerate samples that exhibit high ρ values have a negligible electronic contribution. For the degenerate samples, the temperature dependence of L has been estimated by a single-parabolic-band (SPB) model. The lowest κ_L values achieved, on the order of 0.75 $W\,m^{-1}\,K^{-1}$ up to 500 K, are similar to those obtained in other n- and p-type type-I clathrates. Due to the polycrystalline nature of the present samples that induces grain boundary scattering, these values are consistently lower than those

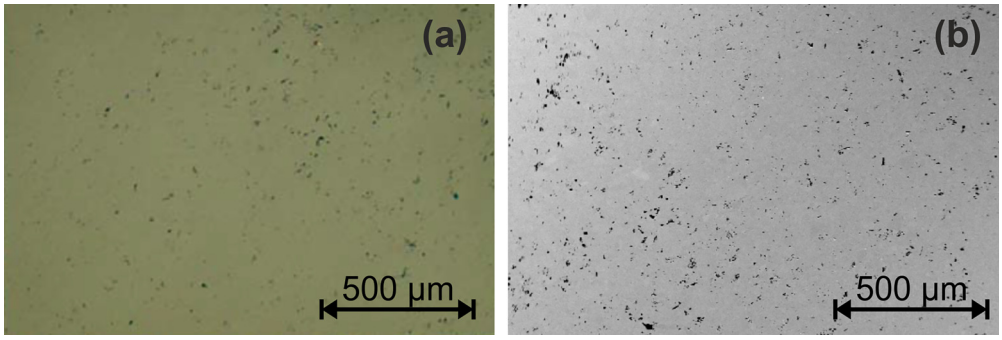

FIG. 2. Microstructure of the sample with nominal composition $Ba_8Au_{5.33}Ge_{40.67}$ manufactured by SPS treatment at 1073 K: (a) optical microscopy image and (b) scanning electron microscopy image (backscattered electron contrast).

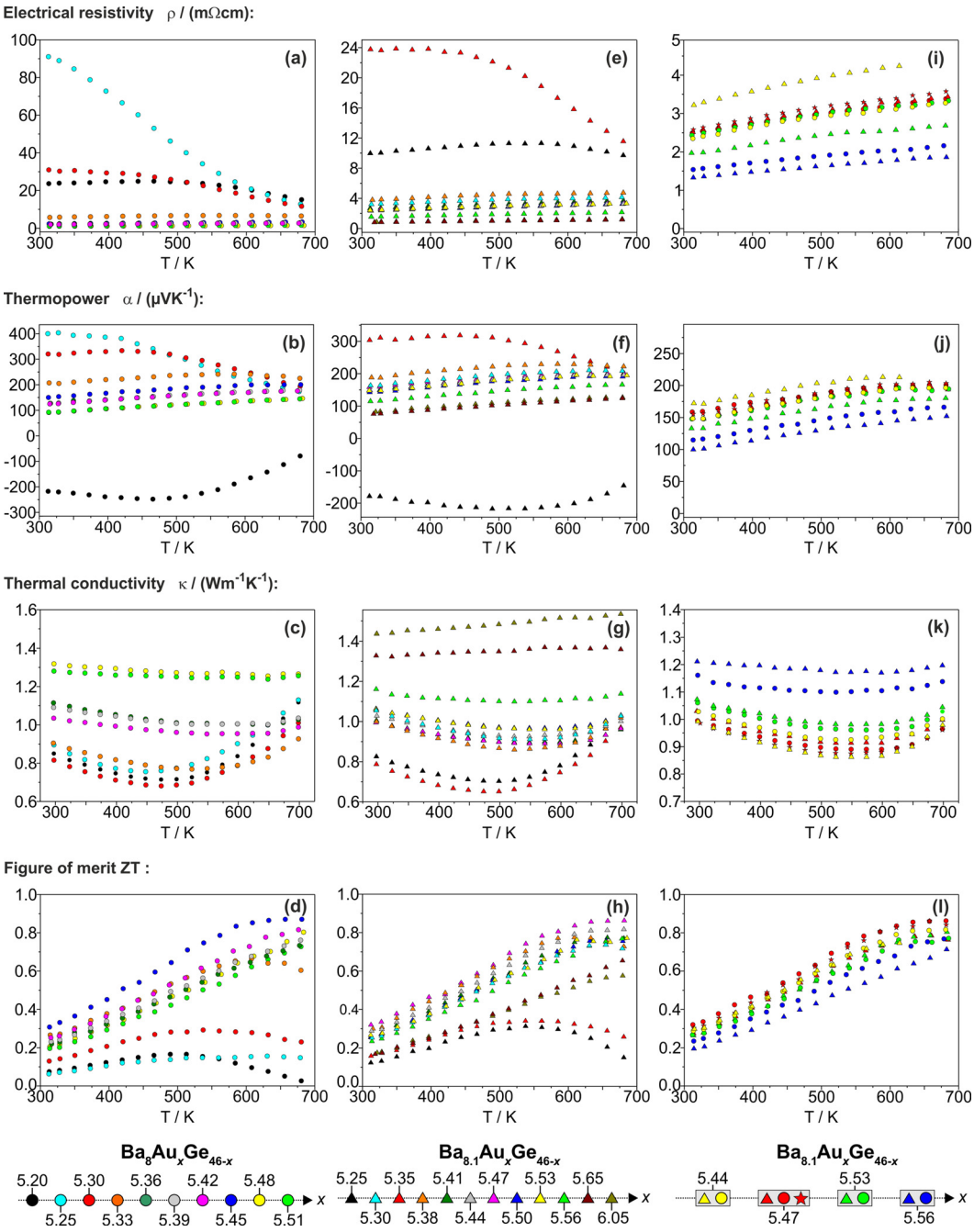

FIG. 3. Temperature dependence of thermoelectric properties between 300 and 700 K. Electrical resistivity ρ, thermopower α, thermal conductivity κ, and the dimensionless thermoelectric figure of merit ZT of samples with nominal compositions $Ba_8Au_xGe_{46-x}$ (a)–(d) and $Ba_{8.1}Au_xGe_{46-x}$ (e)–(h). Reproducibility of the thermoelectric properties for different batches with the same composition in the series $Ba_{8.1}Au_xGe_{46-x}$ (i)–(l).

measured on single-crystalline $Ba_{7.8}Au_{5.33}Ge_{40.67}$ (Ref. 8). Similar values are obtained for both series, indicating that the nature of the secondary phase has little influence on the thermal transport. The high-temperature amorphous limit κ_{Glass} to κ_L is estimated from the relation

$$\kappa_{Glass} = \frac{1}{2}\left(\frac{\pi}{6}\right)^{1/3} k_B V^{-2/3}(2v_T + v_L),$$

where k_B is the Boltzmann constant, V is the average volume per atom, and v_T and v_L are the transverse and longitudinal sound

TABLE II. Characterization of different batches with nominal composition $Ba_{8.1}Au_{5.47}Ge_{40.53}$ after SPS treatment of 12 g of the sample. The amount of phases written in brackets is close to the detection limit of XRPD. Lattice parameter and WDXS composition refer to the clathrate-I phase (C-I).

Batch	Detected phases	Lattice parameter/Å[a]	WDXS composition
01	C-I, α-Ge	10.7966(1)	
02	C-I	10.7985(1)	
03	C-I, (α-Ge)	10.7979(1)	
04	C-I, $BaAu_xGe_{4-x}$	10.7985(1)	$Ba_{8.00(3)}Au_{5.49(2)}Ge_{40.68(3)}$
05	C-I, (α-Ge)	10.7976(1)	
06	C-I, $BaAu_xGe_{4-x}$	10.7982(1)	
08	C-I, $BaAu_xGe_{4-x}$	10.7979(1)	
09	C-I	10.7980(1)	
10	C-I	10.7980(1)	$Ba_{8.0(2)}Au_{5.49(2)}Ge_{40.2(2)}$
11	C-I, α-Ge	10.7971(1)	
12	C-I, (α-Ge)	10.7978(1)	
13	C-I, (α-Ge)	10.7978(1)	$Ba_{8.00(6)}Au_{5.54(5)}Ge_{40.66(5)}$

[a]The lattice parameter was refined with LaB_6 standard and the same set of reflections.

velocities, respectively. Using $v_T = 2930$ and $v_L = 4520$ m s^{-1} inferred from acoustic dispersions measured by inelastic neutron scattering on single-crystalline $Ba_{7.8}Au_{5.33}Ge_{40.67}$,[5] this relation yields $\kappa_{Glass} = 0.12$ W m^{-1} K^{-1}. In none of the samples, this limit is reached at high temperatures, indicating that further reduction in κ_L may be achieved by further alloying to increase point-defect scattering.

Combining the three transport properties, the calculated ZT values increase with temperature to reach a maximum value of ≈0.9 at 670 K [Figs. 3(d) and 3(h)]. This peak value is consistently achieved in both series for Au concentrations falling in the range $5.40 \leq x \leq 5.50$ and is, thus, remarkably robust against minor changes in the chemical composition, which is a favorable characteristic for up-scaling the synthesis process.

To investigate the reproducibility of the preparation process and the ZT values, the preparation and characterization of the series $Ba_{8.1}Au_xGe_{46-x}$ was repeated for the compositions $x = 5.44$, 5.47, 5.53, and 5.56 [Figs. 3(i)–3(l)]. The batches with $x = 5.44$, 5.47, and 5.53, which were weighed with an accuracy of $\Delta m = 0.1$ mg for an overall mass of 3 g, led to fully reproducible transport data. Only the sample $x = 5.56$ with a less accurate weighing of $\Delta m = 1$ mg showed measurable differences in ZT [Fig. 3(l)], which provides an idea about the accuracy required. The sample with $x = 5.47$ achieved the highest thermoelectric performance and was, thus, chosen for an upscaling process and the fabrication of a thermoelectric generator. A 160 g of the precursor material was manufactured by SPS treatment to 13 pellets ($\varnothing = 15$ mm, $l = 9$ mm, $m \approx 12$ g), which were cut to module legs of dimensions $5 \times 5 \times 7$ mm^3. Also in this larger preparation scale, the samples were either single-phase clathrate materials or contained small amounts of $BaAu_{1.1}Ge_{2.9}$ or α-Ge as impurity phases (Table II). The lattice parameter a of the clathrate-I phase was constant within $\Delta a \leq 10^{-3}$ Å. Moreover, wavelength-dispersive x-ray spectroscopy (WDXS) analysis did not show any significant differences for the clathrate composition from sample to sample.

The manufactured legs were tested by electrical resistivity measurements for which contacts were placed at opposite faces of the cuboids (Fig. S3). In this way, samples with microscopic cracks were detected by distinctly higher resistance and separated. For the fabrication of a thermoelectric module suitable for high-temperature application in the region of about 500 °C, traditional soldering materials, such as tin or lead, cannot be used due to their low melting point. For Ge-based clathrates, the additional problem arises that the clathrate phase reacts with most d-elements to form stable binary germanides. Therefore, materials like Fe, Cu, or Ni cannot be used. The result is exemplarily shown for a thin layer of Ni powder, pressed by SPS treatment on the sample. The interface showed cracks, and several Ni-containing phases had formed (Fig. 4). A solution to this problem is the manufacturing of a thin carbon layer acting as a diffusion barrier that separates the clathrate phase from the electrical contacts. As the preparation and the SPS experiment show, carbon does not react with the clathrate phase (Fig. 4).

With the module legs obtained, a thermoelectric test module was manufactured. In the test module, the p-type legs with the nominal composition $Ba_{8.1}Au_{5.47}Ge_{40.53}$ were combined with n-type legs of the $Ba_8Ga_{16}Ge_{30}$ clathrate. Samples of the latter material were prepared

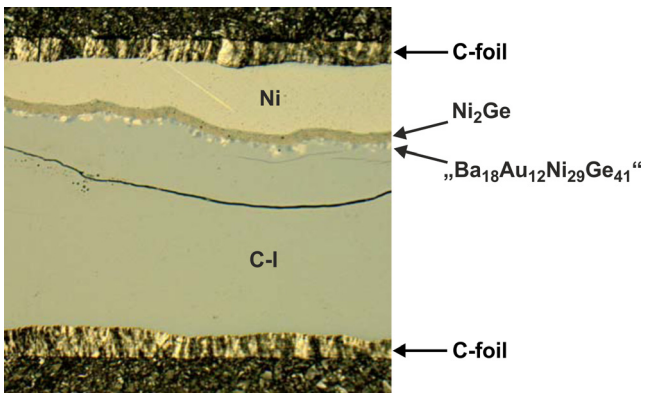

FIG. 4. SPS-sintered Ni layer on a clathrate-I pellet of $Ba_{7.8}Au_{5.33}Ge_{40.67}$. The sample shows cracks, a layer of Ni_2Ge, and an unknown quaternary phase. At the bottom, the carbon layer did not react with the clathrate-I phase.

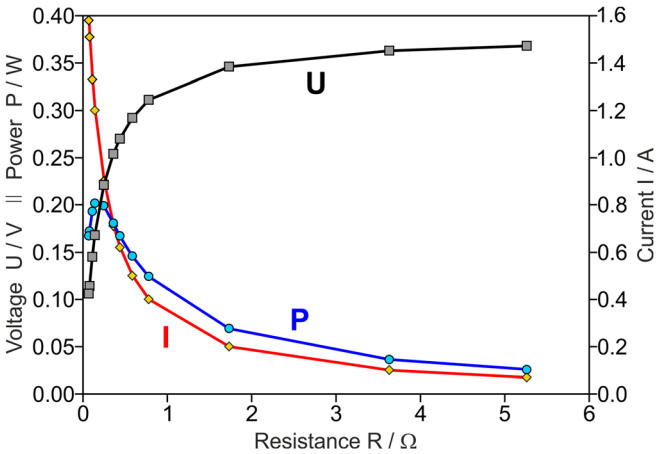

FIG. 5. Current–voltage characteristics for the clathrate-I module for $T_{hot} = 673$ K and $T_{cold} = 293$ K. Electrical voltage and power share the same numeric scale.

with the nominal composition $Ba_8Ga_{15.6}Ge_{30.4}$ using a preparation route similar to the one used for $Ba_{8.1}Au_{5.47}Ge_{40.53}$. For $Ba_8Ga_{15.6}Ge_{30.4}$, a thermoelectric figure of merit $ZT \approx 0.35$ was achieved at 670 K (Fig. S4), which is similar to that reported for $Ba_8Ga_{16}Ge_{30}$.[15] The legs were assembled on the thermal conducting ceramics Rulit708S/Al_2O_3. The module parameters were measured on the specialized high-precision setup. The internal resistance was measured at 1000 Hz frequency and amounted to 148 mΩ at 293 K. The measurement uncertainty of the heat flow through the module was less than 3% and less than 0.3% for the electric module with an external load. Without any optimization of the module assembly, the output power was 0.2 W for cold and hot side temperatures of 293 and 673 K, respectively (Fig. 5). Further optimization is in the scope of future projects.

To conclude, the thermoelectric properties of the type-I clathrate phase $Ba_{8-\delta}Au_xGe_{46-y}$ were investigated for several sample compositions in the region $Ba_{7.8}Au_{5.33}Ge_{40.7}$. A maximum dimensionless thermoelectric figure of merit ZT of ≈0.9 at 670 K was achieved and shown to be highly reproducible. Germanium as a minority phase hardly influences the thermoelectric performance. An upscaling procedure consisting of steel quenching and spark plasma sintering allows the production of a nearly phase pure specimen in a short time without affecting the thermoelectric properties. Module legs were manufactured and integrated into a demonstrator module.

See the supplementary material for microstructure analysis of the clathrate phase, x-ray powder diffraction patterns, electrical resistivity measurements on the fabricated legs, and the temperature-dependent ZT-value of the $Ba_8Ga_{16}Ge_{30}$ sample used for the *n*-type legs of the demonstrator module.

The authors acknowledge financial support within the BMBF project IN-TEG.

DATA AVAILABILITY

The data that support the findings of this study are available from the corresponding author upon reasonable request.

REFERENCES

[1]J. Dolyniuk, B. Owens-Baird, J. Wang, J. V. Zaikina, and K. Kovnir, Mater. Sci. Eng.: R **108**, 1–48 (2016).
[2]*The Physics and Chemistry of Inorganic Clathrates*, Springer Series in Materials Science, edited by G. S. Nolas (Springer, 2014).
[3]J. S. Kasper, P. Hagenmuller, M. Pouchard, and C. Cros, Science **150**, 1713 (1965).
[4]B. Eisenmann, H. Schäfer, and R. Zagler, J. Less-Common Met. **118**, 43 (1986).
[5]P.-F. Lory, S. Pailhès, V. M. Giordano, H. Euchner, H. D. Nguyen, R. Ramlau, H. Borrmann, M. Schmidt, M. Baitinger, M. Ikeda, P. Tomeš, M. Mihalkovič, C. Allio, M. R. Johnson, H. Schober, Y. Sidis, F. Bourdarot, L. P. Regnault, J. Ollivier, S. Paschen, Y. Grin, and M. de Boissieu, Nat. Commun. **8**, 491 (2017).
[6]A. Bhattacharya, C. Carbogno, B. Böhme, M. Baitinger, Y. Grin, and M. Scheffler, Phys. Rev. Lett. **118**, 236401 (2017).
[7]M. Baitinger, B. Böhme, F. R. Wagner, and U. Schwarz, Z. Anorg. Allg. Chem. **646**, 1034 (2020).
[8]H. Zhang, H. Borrmann, N. Oeschler, C. Candolfi, W. Schnelle, M. Schmidt, U. Burkhardt, M. Baitinger, J.-T. Zhao, and Y. Grin, Inorg. Chem. **50**, 1250 (2011).
[9]I. Zeiringer, N. Melnychenko-Koblyuk, A. Grytsiv, E. Bauer, G. Giester, and P. Rogl, J. Phase Equilib. Diffus. **32**, 115 (2011).
[10]H. Anno, M. Hokazone, H. Takakura, and K. Matsubara, in *ICT* (Clemson, 2005), p. 102.
[11]C. Candolfi, U. Aydemir, M. Baitinger, N. Oeschler, F. Steglich, and Y. Grin, J. Electron. Mater. **39**, 2039 (2010).
[12]F. Merlo and M. L. Fornasini, J. Less-Common Met. **13**, 603 (1967).
[13]U. Aydemir, C. Candolfi, A. Ormeci, Y. Oztan, M. Baitinger, N. Oeschler, F. Steglich, and Y. Grin, Phys. Rev. B **84**, 195137 (2011).
[14]C. Candolfi, U. Aydemir, M. Baitinger, N. Oeschler, F. Steglich, and Y. Grin, J. Appl. Phys. **111**, 043706 (2012).
[15]E. S. Toberer, M. Christensen, B. B. Iversen, and G. J. Snyder, Phys. Rev. B **77**, 075203 (2008).